Journal of the European Ceramic Society 39 (2019) 2673–2679

Contents lists available at ScienceDirect

Journal of the European Ceramic Society

journal homepage: www.elsevier.com/locate/jeurceramsoc

Original Article

Enhanced breakdown strength and energy storage density in a new $BiFeO_3$-based ternary lead-free relaxor ferroelectric ceramic

Haoguang Yang, He Qi, Ruzhong Zuo*

Institute of Electro Ceramics & Devices, School of Materials Science and Engineering, Hefei University of Technology, Hefei, 230009, PR China

ARTICLE INFO

Keywords:
Lead-free ceramics
Energy storage
$BiFeO_3$
Relaxor ferroelectrics
BDS

ABSTRACT

A new ternary lead-free relaxor ferroelectric ceramic of (0.67-x)$BiFeO_3$-0.33($Ba_{0.8}Sr_{0.2}$)TiO_3-xLa($Mg_{2/3}Nb_{1/3}$)O_3 + y wt.% MnO_2 + z wt.% $BaCu(B_2O_5)$ (BF-BST-xLMN + y wt.% MnO_2 + z wt.% BCB) was prepared by a solid-state reaction method. The substitution of LMN for BF was believed to induce a typical dielectric relaxation behavior owing to the increased random fields. After co-doping MnO_2 and BCB, a significant decrease in the conductivity and grain size was simultaneously realized, resulting in obviously enhanced dielectric breakdown strength and energy-storage performances at room temperature. A high recoverable energy storage density W~3.38 J/cm^3 and an acceptable energy storage efficiency η~59% were achieved in the composition with x = 0.06, y = 0.1 and z = 2 under a measuring electric field of 23 kV/mm. In addition, the energy-storage performance is quite stable against both frequency (0.1 Hz–100 Hz) and temperature (30–170 °C), suggesting that BF-BST-xLMN + y wt.% MnO_2 + z wt.% BCB lead-free relaxor ferroelectric ceramics might be a promising dielectric material for high-power pulsed capacitors.

1. Introduction

In recent years, dielectric capacitors have received special attention because of higher power density and extremely high charge-discharge speed [1–3]. The recoverable energy storage density (W) and the energy storage efficiency (η) of dielectric capacitors can be given by the following formula:

$$W = \int_{P_r}^{P_{max}} EdP \quad (1)$$

$$W_{loss} = \int PdE \quad (2)$$

$$\eta = W/(W + W_{loss}) \quad (3)$$

where P, P_{max}, and P_r are the polarization under applied electric field strength E, the saturated polarization, and the remanent polarization, respectively, W_{loss} is the area of hysteresis loops [4,5]. Therefore, to get high W and η, both a large polarization difference ΔP (ΔP = P_{max}-P_r), and a high dielectric breakdown strength (BDS) are required. In addition, the temperature stable range is also an essential parameter for the device application. Considering the fact that the polarization of relaxors can exhibit a good temperature stability due to their diffuse phase transition behavior around the dielectric maxima, relaxor ferroelectrics should be attractive in the field of dielectric energy storage [6–8].

Excellent energy-storage properties have been so far reported in a couple of lead-based ferroelectric ceramics [8–11]. However, due to the toxicity of lead, efforts to develop lead-free alternatives are necessary. As a result, $BaTiO_3$ (BT), ($Bi_{1/2}Na_{1/2}$)TiO_3 (BNT), ($K_{0.5}Na_{0.5}$)NbO_3 and $BiFeO_3$ (BF)-based lead-free ceramics have been extensively investigated [12–16]. Among them, BF has attracted increasing attention because of its large spontaneous polarization (P ~ 100 μC/cm^2) [17]. Although BF-BT solid solutions exhibit large P_{max} (> 40 μC/cm^2) and high Curie temperature at the phase boundary between rhombohedral and pseudocubic phases, yet large P_r and high dielectric loss (tan δ) might have increased the difficulty in the research and development in the energy-storage field [18]. Recently, large W values of 1.66–2.56 J/cm^3 were reported in BF-BT based relaxor ferroelectrics by introducing low-loss ABO_3 perovskites, such as La($Mg_{1/2}Ti_{1/2}$)O_3 (LMT) and Bi($Zn_{1/3}Ta_{2/3}$)O_3 (BZT) [19,20]. An obviously enhanced energy storage density owing to higher BDS ~70 kV/mm was achieved in BF-based multilayers with a layer thickness of ~16 μm [21], however, the BDS value (~13–18 kV/mm) of BF-based ceramics is still quite low in comparison with that of other high-performance dielectric ceramics.

Generally, the BDS value of a dielectric ceramic depends on internal factors (density, grain size and grain boundary characteristics) and external factors (sample area, sample thickness and electrode configuration) [22,23]. The large dielectric loss and high conductivity in BF-

* Corresponding author.
E-mail address: piezolab@hfut.edu.cn (R. Zuo).

https://doi.org/10.1016/j.jeurceramsoc.2019.03.001
Received 13 January 2019; Received in revised form 27 February 2019; Accepted 1 March 2019
Available online 02 March 2019

based ceramics were generally believed to be a result of oxygen vacancies caused by the coexisting Fe^{2+} / Fe^{3+}, and low relative densities during sintering, which could be effectively solved by introducing multivalent elements and liquid phases as sintering aids, respectively. [24–26] Therefore, in this work, 0.1 wt.% MnO_2 and different contents of low-melting-point $BaCu(B_2O_5)$ (BCB) were simultaneously added into BF-$(Ba_{0.8}Sr_{0.2})TiO_3$-$La(Mg_{2/3}Nb_{1/3})O_3$ (BF-BST-LMN) lead-free relaxor ferroelectrics. As a result, an enhanced dielectric breakdown property (BDS ~ 23.8 kV/mm) and an excellent recoverable energy storage density (W ~ 3.38 J/cm^3) have been obtained, exhibiting large potentials by comparing those previously reported.

2. Experimental

The (0.67-x)BF-0.33BST-xLMN + y wt.% MnO_2 + z wt.% BCB (BF-BST-xLMN + y wt.% MnO_2 + z wt.% BCB, x = 0-0.08, y = 0, 0.1, z = 1–4) ceramics were fabricated by a conventional solid-state method. Bi_2O_3 (≥99.0%), Fe_2O_3 (≥99.0%), $BaCO_3$ (≥99.0%), TiO_2 (≥99.0%), La_2O_3 (≥99.0%), $(MgCO_3)_4{\cdot}Mg(OH)_2{\cdot}5H_2O$ (≥99.0%), Nb_2O_5 (≥99.0%), MnO_2 (≥99.0%), $Ba(OH)_2{\cdot}8H_2O$ (≥99%), CuO (≥99%) and H_3BO_3 (≥99%) powders (Sinopharm Chemical Reagent Co., Ltd., CN) were used as the starting materials. The BF-BST-xLMN powder was first synthesized through calcination at 700–800 °C. After that, the BCB powder was prepared by mixing the stoichiometric powders and then calcinating the dried powder mixture at 810 °C for 4 h. Finally, 0.1 wt.% MnO_2 and different contents of BCB powder were added into the as-synthesized BF-BST-xLMN powder through ball milling together with 0.5 wt.% PVB binder. The sample discs were sintered at 920–1020 °C in a sacrificial powder of the same composition in closed crucibles. The ceramic samples for measuring electrical properties were well polished to obtain parallel surfaces and painted with silver paste and then fired at 550 °C for 30 min.

The phase structure of ceramics powders was determined by powder X-ray diffraction (XRD, D/Max-RB, Rigaku, Tokyo, Japan) with Cu Kα radiation. The XRD spectra were measured in 2θ range from 20° to 60° with a step size of 0.02° and a scanning speed of 10°/min. The relative density was estimated by the Archimedes method. The grain morphology was observed by field emission scanning electron microscopy (FE-SEM, SU8020, JEOL, Tokyo, Japan). Before the SEM observation, the samples were polished and then thermally etched for 20 min at 800 °C. The dielectric constant and loss of fresh (unpoled) samples were measured by an LCR meter (Agilent E4980 A, Santa Clara, CA) as a function of temperature (30–550 °C) and frequency (10 kHz-1 MHz). Electric field-induced polarization (P-E) hysteresis loops were measured using a ferroelectric measurement system with a triangular signal of 10 Hz (Precision multi-ferroelectric, Radiant Technologies Inc, Albuquerque, NM). The impedance spectra at 280 °C and the dielectric loss at room temperature (RT) were measured by a dielectric testing system (Novocontrol Technologies, GmbH, Germany) over a frequency range from 1 Hz to 1 MHz with an AC voltage of 1 V. The BDS value was measured using a voltage breakdown tester (BDJC-50 kV, Beijing Beiguang Jingyi Instrument Equipment Co. Ltd, Beijing, China). During the BDS test, at least 10 samples were used for each composition. A DC voltage rising rate of about 1 kV/s was applied to each sample till the dielectric breakdown. For P-E and BDS measurements, the thickness and diameter of the samples were finished into ~ 0.3 mm and ~ 8 mm, respectively. All samples used for the measurement were sintered at their optimum temperatures.

3. Results and discussion

Fig. 1(a) illustrates the RT XRD patterns of BF-BST-xLMN ceramics. All samples show a single perovskite structure without any secondary phase, and have a pseudocubic symmetry because of no splitting of both (111) and (200) diffraction peaks, as shown in Fig. 1(b). It can be observed that the (111) and (200) reflection peaks shift toward higher diffraction angles with increasing LMN content, corresponding to the decrease of lattice parameters and cell volumes, as illustrated in Fig. 1(c). This may be due to the fact that the radius of La^{3+} (CN = 12, $R_{La}{}^{3+}$ = 1.22 Å) is smaller than that of Bi^{3+} (CN = 12, $R_{Bi}{}^{3+}$ = 1.42 Å), although the average radius of complex ions $(Mg_{2/3}Nb_{1/3})^{3+}$ (CN = 6, $R_{(Mg2/3Nb1/3)}{}^{3+}$ = 0.693 Å) is larger than that of Fe^{3+} (CN = 6, $R_{Fe}{}^{3+}$ = 0.645 Å) [12,19].

The dielectric constant ε_r and dielectric loss tan δ of several selected BF-BST-xLMN compositions in the frequency range of 10 kHz to 1 MHz are illustrated in Fig. 2(a). With increasing LMN content, the corresponding temperature (T_m) at the dielectric maximum (ε_m) decreases. Furthermore, the dielectric peaks become more diffuse and more frequency dependent, which agrees well with the typical characteristic of relaxor ferroelectrics. The dielectric relaxation characteristics of BF-BST-xLMN ceramics can be described by two parameters γ [27] and ΔT_{relax} [28], in which γ can be calculated by a modified Curie-Weiss law $1/\varepsilon_r - 1/\varepsilon_m = (T-T_m)^{\gamma}/C$ ($T > T_m$), and ΔT_{relax} can be defined as the difference between two T_m values measured at 1 MHz and 10 kHz, respectively. As shown in Fig. 2(b), these two parameters enhance significantly with increasing x, indicating the enhancement of dielectric relaxation behavior. This would be attributed to the increase of the random local field as a result of the disordered distribution of different ions at A and B sites of the ABO_3 lattice. A freezing temperature T_f can be obtained by fitting the measured dielectric permittivity versus temperature curves to the Vogel-Fulcher relationship [28], as shown in the inset of Fig. 2(a), indicating that the relaxor phase at RT transforms from a nonergodic state to an ergodic sate and the x = 0.06 sample exhibits a coexistence of nonergodic and ergodic relaxor state at RT.

P-E loops of BF-BST-xLMN ceramics measured at 9 kV/mm at RT are illustrated in Fig. 2(c). The P_r, ΔP and P_{max} of BF-BST-xLMN ceramics as a function of LMN content are summarized in the inset of Fig. 2(c). The x = 0 ceramic exhibits a saturated P-E loop with relatively large P_{max} and P_r values simultaneously, corresponding to a typical feature of the normal ferroelectric [29]. With increasing LMN content, the P-E loops become slimmer and slimmer. Both P_{max} and P_r decrease owing to the increase of dielectric relaxation. The ΔP increases at first, and then reaches up to a maximum value of ~ 20 μC/cm^2 at x = 0.04-0.06. In addition, W, W_{loss} and η as a function of x are shown in Fig. 2(d). As x increases, the η value increases monotonously. Furthermore, the W value enhances sharply firstly and reaches up to a maximum at x = 0.04-0.06. W_{loss} decreases rapidly with an increase of x. Therefore, BF-BST-0.06LMN ceramic was chosen for further modification research work owing to its optimum energy-storage performance.

Fig. 3(a) shows the impedance spectra of BF-BST-0.06LMN + y wt.% MnO_2 + z wt.% BCB ceramics measured at 280 °C. It can be seen that all impedance spectra nearly exhibit a single semicircular arc, indicating that the contribution of electrical process mainly comes from the grain interior [30]. Moreover, the increased grain resistivity suggests that the addition of a few amount of MnO_2 and BCB can effectively improve the insulation properties of BF-BST-0.06LMN ceramics. A spectroscopic plot of impedance Z'' and electric modulus M'' at 280 °C for y = 0.1, z = 2 is shown in the inset of Fig. 3(a). Only one peak can be observed, indicating that the grains in the ceramics are electrically homogeneous. The data may be interpreted on an equivalent circuit of a single parallel resistor-capacitor (RC) element that is attributed to a single bulk component with a capacitance~3.8×10^{-10} F·cm^{-1} and a resistivity of 14 MΩ cm [21]. In addition, the addition of 0.1 wt.% MnO_2 was found to obviously reduce the tan δ value, as shown in Fig. 3(b). This may be due to the instability of Mn^{4+} ions at high temperature. Higher-valence Mn ions can absorb electrons and evolve into lower-valence Mn^{3+} and Mn^{2+} ions in the sintering process, thus inhibiting the $Fe^{3+} \rightarrow Fe^{2+}$ reaction. By comparison, the addition of BCB shows a negligible effect on the dielectric loss.

The SEM images of BF-BST-0.06LMN + y wt.% MnO_2 + z wt.% BCB ceramics are shown in Fig. 4. It can be seen that all compositions have been well densified. According to the SEM images, the average grain

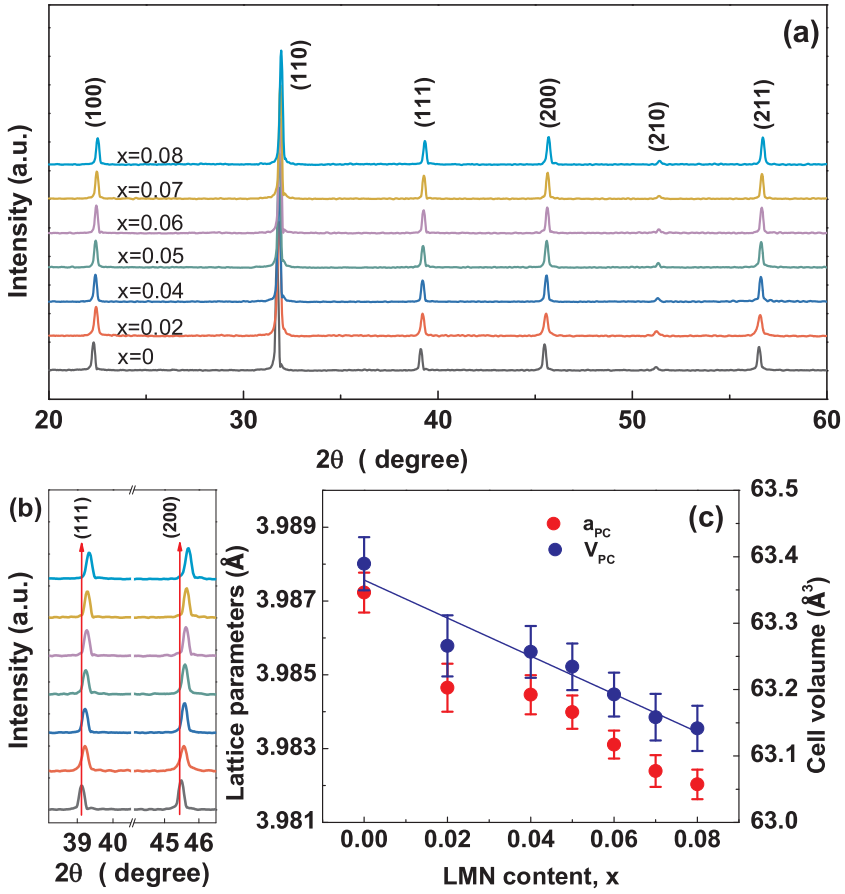

Fig. 1. (a) XRD patterns of BF-BST-xLMN ceramics, (b) local amplification of (111) and (200) diffraction peaks and (c) lattice parameters and cell volumes as a function of x.

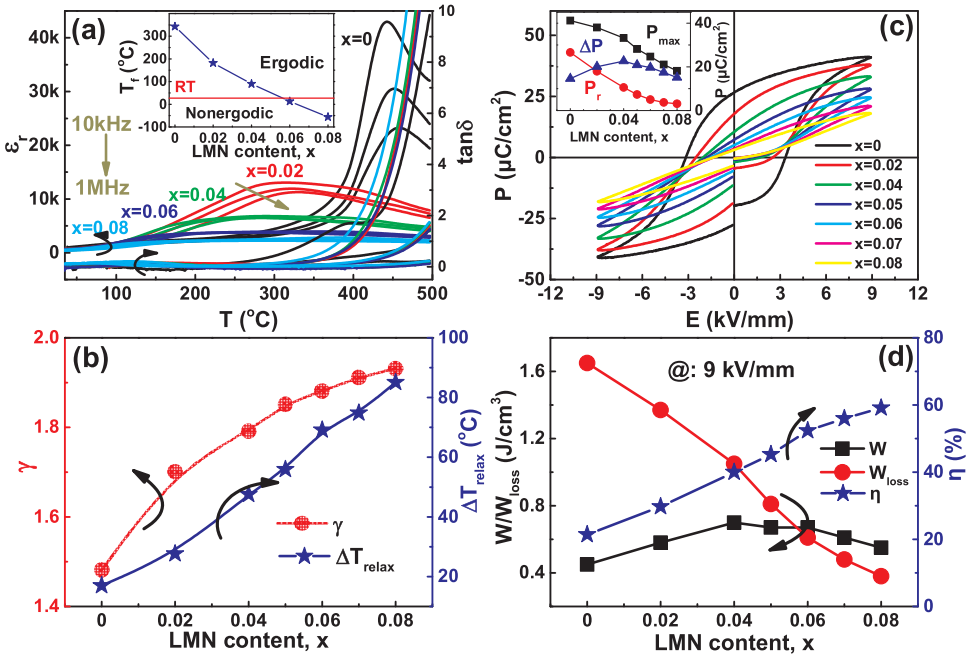

Fig. 2. (a) Temperature dependence of ε_r and tan δ for BF-BST-xLMN ceramics, (b) the variation of γ and ΔT_{relax} as a function of x, (c) P-E loops of BF-BST-xLMN ceramics, and (d) W, W_{loss} and η values as a function of x at 9 kV/mm; the freezing temperature T_f as a function of x is shown in the inset of (a), and P_{max}, P_r, and ΔP values as a function of x at 9 kV/mm is shown in the inset of (c).

size can be estimated, as shown in Fig. 5(a) together with the relative density as a function of MnO_2 and BCB content. It can be seen that with doping 0.1 wt.% MnO_2, the grain size slightly decreases. With further doping BCB, the grain size of the samples decreases significantly. This should be primarily due to the fact that BCB formed a large amount of liquid phase at the grain boundary during sintering, which is similar to the effect of introducing a glass phase [7,31]. In addition, the reduction of sintering temperature due to the liquid-phase sintering mechanism may also help reduce the grain size.

As shown in Fig. 5(b), the values of BDS can be evaluated by means

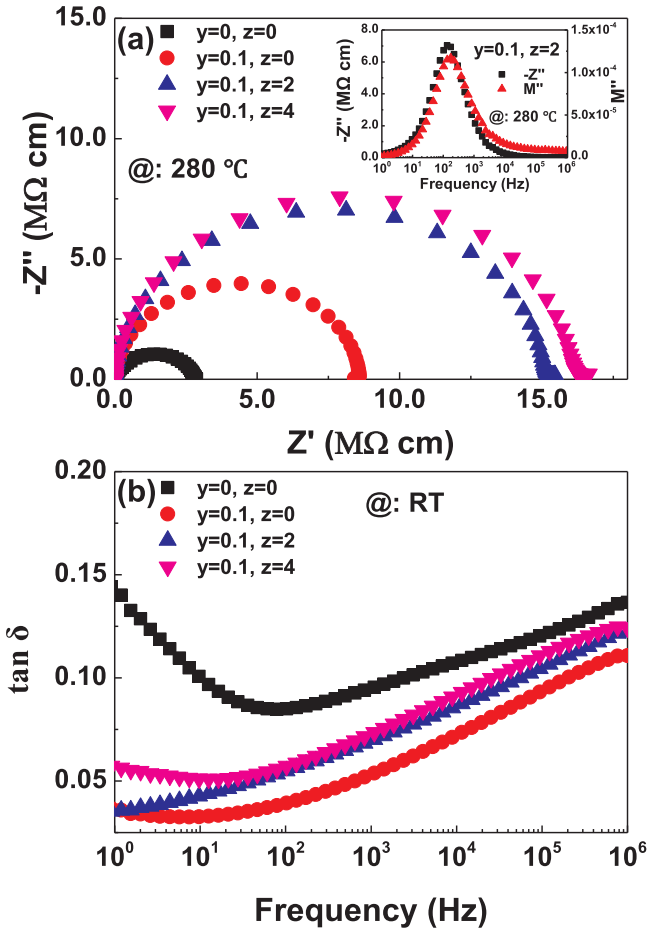

Fig. 3. (a) Impedance spectra of BF-BST-0.06LMN + y wt.% MnO_2 + z wt.% BCB ceramics; the spectroscopic plot of Z" and M" for y = 0.1 and z = 2 at 280 °C is shown in the inset of (a), and (b) frequency dependence of tan δ at RT for BF-BST-0.06LMN + y wt.% MnO_2 + z wt.% BCB ceramics.

of the Weibull distribution functions as follows [22,32,33]:

$$X_i = \ln(E_i) \quad (4)$$

$$Y_i = \ln(\ln(1/(1-p))) \quad (5)$$

$$P_i = i/(n+1) \quad (6)$$

where X_i, Y_i, and P_i are the variables of the Weibull distribution functions, E_i is the measured dielectric breakdown strength for the ith specimen in the experiments and n is the sum of the specimens for each composition. Usually, X_i and Y_i were linearly dependent. The Weibull modulus (m) is the slope of the line, representing the credence of the statistic results. In this case, the m value was higher than 8 for all the components, implying that the effective comparison of feature in BDS is reliable. The average BDS value can be extracted according to the intersection point of the x-axis and the fitting line, as shown in Fig. 5(b). Because the same external parameters were retained for the BDS measurement in this work, the increase of BDS should be mainly ascribed to the decreased grain size and the increased density, as shown in Fig. 5(a). The relationship between BDS and grain size (d) was reported to obey the following relation: $BDS \propto d^{-0.5}$ [34]. The BDS value reaches 23.8 kV/mm as y = 0.1 and z = 2, which is about 1.7 times that of the undoped BF-BST-0.06LMN sample.

Fig. 6(a) shows P-E hysteresis loops of BF-BST-0.06LMN + y wt.% MnO_2 + z wt.% BCB ceramics under an external electric field dose to each BDS value. With increasing the electric field, P_{max} increases significantly, while P_r remains small. Therefore, ΔP increases with increasing the field magnitude (see Fig. 6(b)). As shown in Fig. 6(b) and (c), the BF-BST-0.06LMN ceramic has small ΔP and W under a low electric field (13 kV/mm), which are 27.5 μC/cm^2 and 1.3 J/cm^3, respectively. The BF-BST-0.06LMN + 0.1 wt.% MnO_2 ceramic obtains a larger ΔP of ~ 29.6 μc/cm^2 and W of ~ 1.94 J/cm^3 at 16 kV/mm. This is because that MnO_2 doping could reduce the dielectric loss and increase the resistivity (see Fig. 3), causing the increase of BDS. Even though obvious improvement of the BDS was realized with increasing BCB content (see Fig. 5), P_{max} was found to decrease monotonously owing to the weakening of ferroelectricity. As a result, the largest W ~ 3.38 J/cm^3 was achieved in the BF-BST-0.06LMN + 0.1 wt.% MnO_2 + 2 wt.% BCB ceramic under 23 kV/mm. Fig. 6(d) shows the η value of various ceramics with changing electric field. A moderate η ~ 59% was obtained as y = 0.1 and z = 2 under 23 kV/mm. Generally speaking, ΔP and BDS are two key factors to realize high energy storage density of dielectric capacitors. The introduction of a small amount of BCB liquid phase during sintering tends to reduce the ΔP, but can greatly improve the

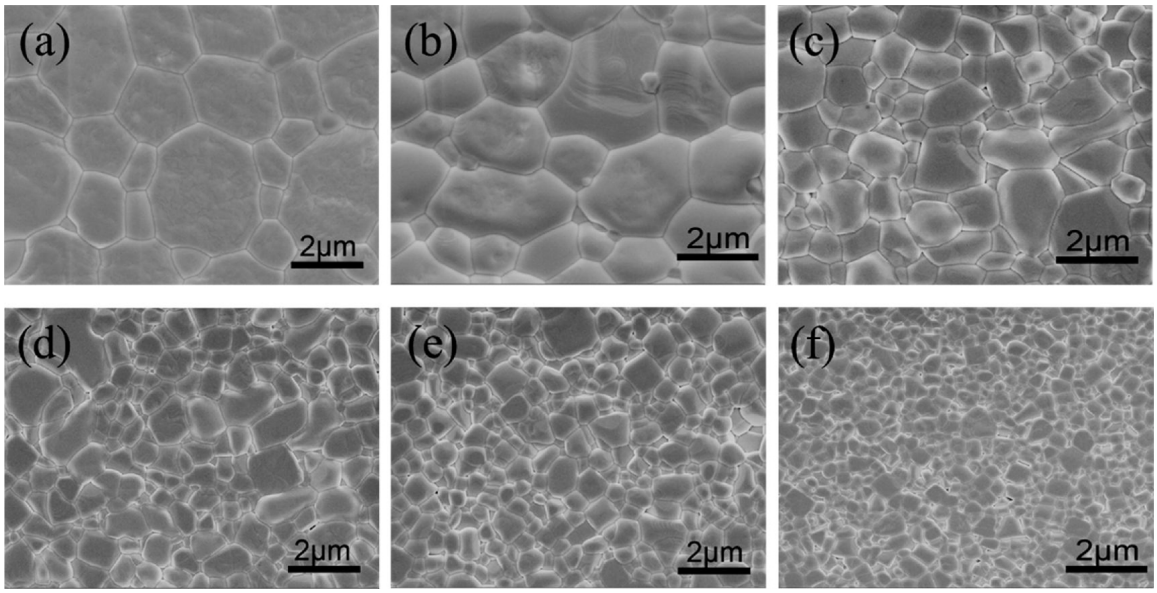

Fig. 4. SEM images of BF-BST-0.06LMN + y wt.% MnO_2 + z wt.% BCB ceramic samples sintered at their optimum temperatures: (a) y = 0, z = 0, (b) y = 0.1, z = 0, (c) y = 0.1, z = 1, (d) y = 0.1, z = 2, (e) y = 0.1, z = 3, (f) y = 0.1, z = 4.

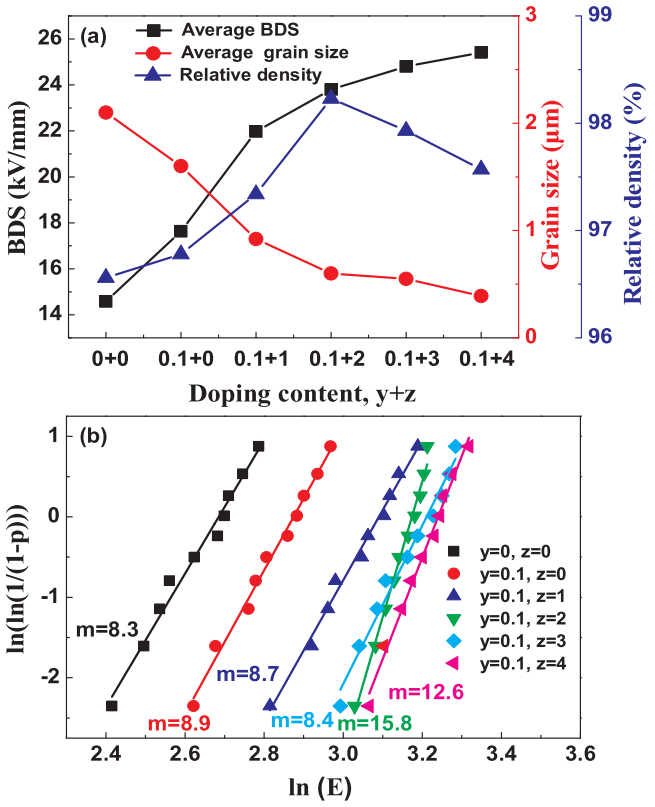

Fig. 5. (a) The BDS, grain size and relative density as a function of y + z, and (b) the Weibull distribution of the BDS for BF-BST-0.06LMN + y wt.% MnO_2 + z wt.% BCB ceramics.

BDS. Therefore, as long as the amount of liquid phase is appropriate, an optimal balance between ΔP and BDS can be achieved. A comparison of polarization and recoverable energy-storage properties among several Bi-containing perovskite ferroelectric systems is displayed in Table 1 [19,20,28,35–39]. It can be seen that the BF-BST-0.06LMN + 0.1 wt.% MnO_2 + 2 wt.% BCB ceramics possess a much higher BDS value together with a much larger W value.

Table 1
A comparison of polarization and recoverable energy-storage properties of Bi-containing perovskite ferroelectric ceramics.

Compounds	E (kV/cm)	P_{max} (μC/cm^2)	ΔP μC/cm^2)	W (J/cm^3)	η (%)	Ref.
BKT-LMT (HP)	18	–	–	2.08	68	35
BNKLSTT (HP)	14.3	–	–	2.42	–	36
BF-BT-Nb_2O_5	9	25	19.7	0.71	–	37
BF-BT-BMN	12.5	38	32.3	1.56	75	27
BF-BT-LMT	13	37.5	33.3	1.66	82	19
BNF-BT	17	39.8	30.7	1.82	41.3	38
BF-BT-BZN	18	36.7	32.8	2.06	53	39
BF-BT-BZT	16	–	43.4	2.56	–	20
BF-BST-LMN-MnO_2-BCB	23	44.1	36.5	3.38	59	This work

BKT: $(Bi_{0.5}K_{0.5})TiO_3$, HP: Hot-press sintering, BNKLSTT: $(Bi_{0.5}[(Na_{0.8}K_{0.2})_{0.90}Li_{0.10}]_{0.5})_{0.96}$-$Sr_{0.04}(Ti_{0.975}Ta_{0.025})O_3$, BMN: $Ba(Mg_{1/3}Nb_{2/3})O_3$, BNF: $(Bi_{1-x}Nd_x)FeO_3$, BZN: $Bi(Zn_{2/3}Nb_{1/3})O_3$.

The stability of energy-storage performance in a wide operating temperature and frequency range is considered as an important criterion for evaluating the performance of energy-storage materials. The temperature and frequency dependence of the energy-storage performances of the BF-BST-0.06LMN + 0.1 wt.% MnO_2 + 2 wt.% BCB ceramic is shown in Fig. 7. It can be seen that the studied ceramic has an excellent energy-storage property stability at 13 kV/mm in the frequency range of 0.1–100 Hz and temperature range of 30–170 °C. As can be seen from Fig. 7(a), with the increase of measuring frequency, the P-E loops become slightly fatter, indicating a slight decrease of the ΔP and a slight increase of the hysteresis loss. This small change should be mainly attributed to the time effect of electric field induced long-range ferroelectric state returning to the initial ergodic state [40,41]. Therefore, W, η and ΔP decrease slightly with increasing frequency, as shown in Fig. 7(b). In addition, the content of non-ergodic relaxor phase decreases gradually with increasing temperature until the sample enters into a complete ergodic relaxor phase region at the high temperature. As seen in Fig. 7(c), a slight increase of P_{max} was observed

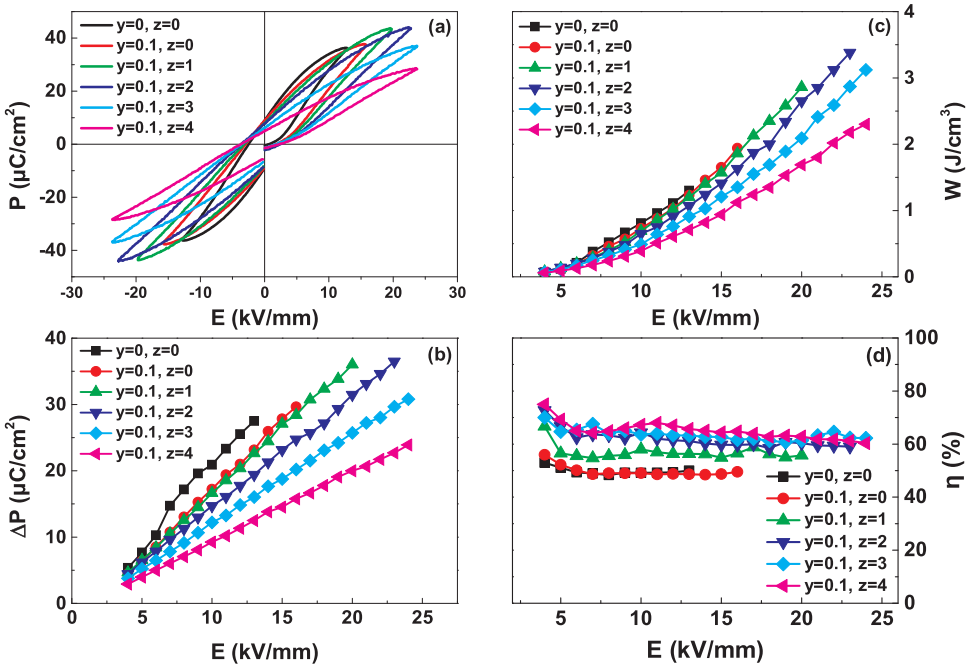

Fig. 6. (a) P-E loops measured under different electric fields at 10 Hz for BF-BST-0.06LMN + y wt.% MnO_2 + z wt.% BCB ceramics, (b) ΔP, (c) W and (d) η values of BF-BST-0.06LMN + y wt.% MnO_2 + z wt.% BCB ceramics.

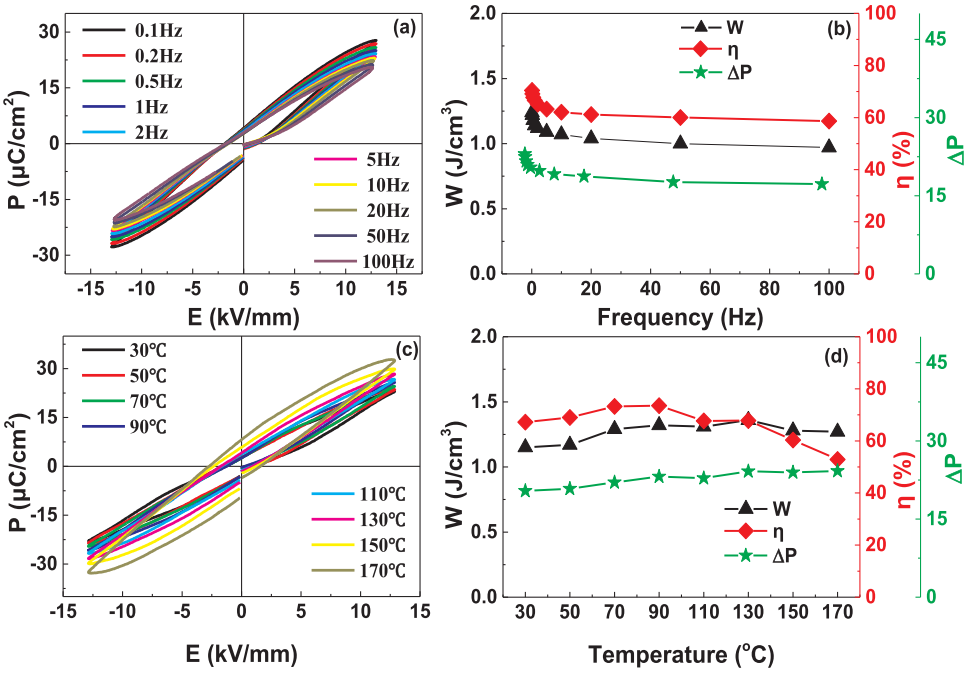

Fig. 7. (a) P-E loops of the BF-BST-0.06LMN + 0.1 wt.% MnO_2 + 2 wt.% BCB ceramic sample measured at RT in the frequency range of 0.1–100 Hz, and (b) the calculated W, η and ΔP values as a function of frequency, (c) P-E loops of the BF-BST-0.06LMN + 0.1 wt.% MnO_2 + 2 wt.% BCB ceramic sample measured at 10 Hz in the temperature range of 30–170 °C, and (d) the calculated W, η and ΔP values as a function of temperature.

with increasing temperature. When the measuring temperature rises from 30 to 170 °C, the ΔP value varies slightly from 20.4 to 24.2 μC/cm^2, due to both the decrease in the nonergodic phase content and the increase in dynamics of polar nanoregions (PNRs). For the same reason, the calculated W value fluctuates slightly between 1.15 and 1.27 J/cm^3 in a wide temperature range, as shown in Fig. 7(d). However, with the increase of temperature, the η value changes from 67% to 53%. On the one hand, the reduction of the non-ergodic phase content would lead to the lack of domain reorientation in the discharge process. On the other hand, the increase of ergodic PNR dynamics should greatly reduce the hysteresis effect of the field-induced ferroelectric phase back to ergodic phases. Nevertheless the BF-BST-0.06LMN + 0.1 wt.% MnO_2 + 2 wt.% BCB ceramic exhibits a good stability against temperature and frequency, indicating a large potential for applications.

4. Conclusions

Enhanced energy-storage properties were realized in BF-BST-LMN lead-free relaxor ferroelectric ceramics doped with MnO_2 and BCB by improving the BDS values as a result of the reduced dielectric loss and grain size. After adding 0.1 wt.% MnO_2 and 2 wt.% BCB, the BDS of the samples is 1.7 times as high as that of undoped BF-BST-LMN ceramics, and the ΔP is raised to 36.5 μC/cm^2. The BF-BST-0.06LMN samples doped with 0.1 wt.% MnO_2 and 2 wt.% BCB liquid phase exhibit the highest recoverable energy-storage density of 3.38 J/cm^3, which is 2.6 times as high as that of undoped BF-BST-0.06LMN ceramics. Moreover, the good recoverable energy-storage properties of W ~ 1.15–1.27 J/cm^3 and η ~ 67%–53% remain stable at 13 kV/mm in the temperature range of 30–170 °C and frequency range of 0.1–100 Hz. The results indicate that BF-BST-LMN ceramics modified with MnO_2 and BCB are promising candidates for high-power pulsed capacitors.

Acknowledgement

This work was supported by the National Natural Science Foundation of China (Grants No. 51472069).

References

[1] X.H. Hao, A review on the dielectric materials for high energy-storage application, J. Adv. Dielect. 03 (2013) 1330001.
[2] L.E. Cross, Relaxor ferroelectrics: an overview, Ferroelectrics 151 (1994) 305–320.
[3] G.R. Love, Energy storage in ceramic dielectrics, J. Am. Ceram. Soc. 73 (1990) 323–328.
[4] S. Kwon, W. Hackenberger, E. Alberta, E. Furman, M. Lanagan, Nonlinear dielectric ceramics and their applications to capacitors and tunable dielectrics, IEEE Electr. Insul. Mag. 27 (2011) 43–55.
[5] Z.H. Yao, Z. Song, H. Hao, Z.Y. Yu, M.H. Cao, S.J. Zhang, M.T. Lanagan, H.X. Liu, Homogeneous/inhomogeneous-structured dielectrics and their energy-storage performances, Adv. Mater. 29 (2017) 1601727.
[6] Y.L. Wang, X.L. Chen, H.F. Zhou, L. Fang, L.J. Liu, H. Zhang, Evolution of phase transformation behavior and dielectric temperature stability of $BaTiO_3$-Bi$(Zn_{0.5}Zr_{0.5})O_3$ ceramics system, J. Alloys. Compd. 551 (2013) 365–369.
[7] X.R. Wang, Y. Zhang, X.Z. Song, Z.B. Yuan, Tao. Ma, Q. Zhang, C.S. Deng, T.X. Liang, Glass additive in barium titanate ceramics and its influence on electrical breakdown strength in relation with energy storage properties, J. Eur. Ceram. Soc. 32 (2012) 559–567.
[8] F. Bian, S.G. Yan, C.H. Xu, Z. Liu, X.F. Chen, C.L. Mao, F. Cao, J.J. Bian, G.S. Wang, X.L. Dong, Enhanced breakdown strength and energy density of antiferroelectric Pb,La(Zr,Sn,Ti)O_3, ceramic by forming core-shell structure, J. Eur. Ceram. Soc. 38 (2018) 3170–3176.
[9] Z.Q. Hu, B.H. Ma, R.E. Koritala, U. Balachandran, Temperature-dependent energy storage properties of antiferroelectric $Pb_{0.96}La_{0.04}Zr_{0.98}Ti_{0.02}O_3$ thin films, Appl. Phys. Lett. 104 (2014) 263902.
[10] Q.F. Zhang, H.F. Tong, J. Chen, Y.M. Lu, T.Q. Yang, X. Yao, Y.B. He, High recoverable energy density over a wide temperature range in Sr modified (Pb,La)(Zr,Sn,Ti)O_3 antiferroelectric ceramics with an orthorhombic phase, Appl. Phys. Lett. 109 (2016) 262901.
[11] L. Zhang, S.L. Jiang, B.Y. Fan, G.Z. Zhang, Enhanced energy storage performance in $(Pb_{0.858}Ba_{0.1}La_{0.02}Y_{0.008})(Zr_{0.65}Sn_{0.3}Ti_{0.05})O_3$-$(Pb_{0.97}La_{0.02})(Zr_{0.9}Sn_{0.05}Ti_{0.05})O_3$ anti-ferroelectric composite ceramics by spark plasma sintering, J. Alloys. Compd. 622 (2015) 162–165.
[12] T. Wang, L. Jin, C.C. Li, Q.Y. Hu, X.Y. Wei, Relaxor ferroelectric $BaTiO_3$-Bi$(Mg_{2/3}Nb_{1/3})O_3$ ceramics for energy storage application, J. Am. Ceram. Soc. 98 (2015) 559–566.
[13] Q. Xu, J. Xie, Z.C. He, L. Zhang, M.H. Cao, X.D. Huang, M.T. Lanagan, H. Hao, Z.H. Yao, H.X. Liu, Energy-storage properties of $Bi_{0.5}Na_{0.5}TiO_3$-$BaTiO_3$-$KNbO_3$ ceramics fabricated by wet-chemical method, J. Eur. Ceram. Soc. 37 (2017) 99–106.
[14] Q. Xu, H.X. Liu, L. Zhang, J. Xie, H. Hao, M.H. Cao, Z.H. Yao, M.T. Lanagan, Structure and electrical properties of lead-free $Bi_{0.5}Na_{0.5}TiO_3$-based ceramics for energy-storage applications, RSC Adv. 6 (2016) 59280.
[15] Z.T. Yang, H.L. Du, S.B. Qu, Y.D. Hou, H. Ma, J.F. Wang, J. Wang, X.Y. Wei, Z. Xu, Significantly enhanced recoverable energy storage density in potassium-sodium niobate-based lead free ceramics, J. Mater. Chem. A 4 (2016) 13778–13785.
[16] T.Q. Shao, H.L. Du, H. Ma, S.B. Qu, J. Wang, J.F. Wang, X.Y. Wei, Z. Xu, Potassium-sodium niobate based lead-free ceramics: novel electrical energy storage materials, J. Mater. Chem. A 5 (2017) 554–563.
[17] D. Lebeugle, D. Colson, A. Forget, M. Viret, Very large spontaneous electric polarization in $BiFeO_3$ single crystals at room temperature and its evolution under cycling fields, Appl. Phys. Lett. 91 (2007) 022907.
[18] T. Ozaki, S. Kitagawa, S. Nishihara, Y. Hosokoshi, M. Suzuki, Y. Noguchi, M. Miyayama, S. Mori, Ferroelectric properties and nano-scaled domain structures

in (1-x)$BiFeO_3$-x$BaTiO_3$ (0.33 < x < 0.50), Ferroelectrics 385 (2009) 155–161.
[19] D.G. Zheng, R.Z. Zuo, Enhanced energy storage properties in La($Mg_{1/2}Ti_{1/2}$)O_3-modified $BiFeO_3$-$BaTiO_3$ lead-free relaxor ferroelectric ceramics within a wide temperature range, J. Eur. Ceram. Soc. 37 (2017) 413–418.
[20] N.T. Liu, R.H. Liang, Z.Y. Zhou, X.L. Dong, Designing lead-free bismuth ferrite-based ceramics learning from relaxor ferroelectric behavior for simultaneous high energy density and efficiency under low electric field, J. Mater. Chem. C 6 (2018) 10211–10217.
[21] G. Wang, J.L. Li, X. Zhang, Z.M. Fan, F. Yang, A. Feteira, D. Zhou, D.C. Sinclair, T. Ma, X.L. Tan, D.W. Wang, I.M. Reane, Ultrahigh energy storage density lead-free multilayers by controlled electrical homogeneity, Energy Environ. Sci. 12 (2019) 582–588.
[22] J.J. Huang, Y. Zhang, T. Ma, H.T. Li, L.W. Zhang, Correlation between dielectric breakdown strength and interface polarization in barium strontium titanate glass ceramics, Appl. Phys. Lett. 96 (2010) 042902.
[23] J.C. Chen, Y. Zhang, C.S. Deng, X.M. Dai, Effect of the Ba/Ti ratio on the microstructures and dielectric properties of barium titanate-based glass-ceramics, J. Am. Ceram. Soc. 92 (2009) 1350–1353.
[24] S.O. Leontsev, R.E. Eitel, Dielectric and piezoelectric properties in Mn-modified (1 − x)$BiFeO_3$-x$BaTiO_3$ ceramics, J. Am. Ceram. Soc. 92 (2009) 2957–2961.
[25] Q. Li, J.R. Cheng, J.G. Chen, Reduced dielectric loss and enhanced piezoelectric properties of Mn modified 0.71$BiFeO_3$-0.29$BaTiO_3$ ceramics sintered under oxygen atmosphere, J. Mater. Sci. Mater. Electron 28 (2017) 1370–1377.
[26] H.B. Yang, C.R. Zhou, X.Y. Liu, Q. Zhou, G.H. Chen, W.Z. Li, H. Wang, Piezoelectric properties and temperature stabilities of Mn- and Cu-modified $BiFeO_3$-$BaTiO_3$ high temperature ceramics, J. Eur. Ceram. Soc. 33 (2013) 1177–1183.
[27] K. Uchino, S. Nomura, Critical exponents of the dielectric constants in diffused-phase-transition crystals, Ferroelectrics 44 (1982) 55–61.
[28] D.G. Zheng, R.Z. Zuo, D.S. Zhang, Y. Li, Novel $BiFeO_3$-$BaTiO_3$-Ba($Mg_{1/3}Nb_{2/3}$)O_3 lead-free relaxor ferroelectric ceramics for energy-storage capacitors, J. Am. Ceram. Soc. 98 (2015) 2692–2695.
[29] A.A. Bokov, Z.G. Ye, Recent progress in relaxor ferroelectrics with perovskite structure, J. Mater. Sci. 41 (2006) 31–52.
[30] H.B. Zhang, P.W. Xu, E. Patterson, J.D. Zang, S.L. Jiang, J. Rödel, Preparation and enhanced electrical properties of grain-oriented ($Bi_{1/2}Na_{1/2}$)TiO_3-based lead-free incipient piezoceramics, J. Eur. Ceram. Soc. 35 (2015) 2501–2512.
[31] H.B. Yang, F. Yan, Y. Lin, T. Wang, Enhanced energy storage properties of $Ba_{0.4}Sr_{0.6}TiO_3$ lead-free ceramics with Bi_2O_3-B_2O_3-SiO_2 glass addition, J. Eur. Ceram. Soc. 38 (2018) 1367–1373.
[32] W. Weibull, A statistical distribution function of wide applicability, J. Appl. Mech. (1951) 293–297.
[33] S. Naderi, J.P. Heath, J.S. Dean, Morphology characterisation of inclusions to predict the breakdown strength in electro-ceramic materials: microstructure modeling, Ceram. Int. 45 (2019) 361–368.
[34] T. Tunkasiri, G. Rujijanagul, Dielectric strength of fine grained barium titanate ceramics, J. Mater. Sci. Lett. 15 (1996) 1767–1769.
[35] F. Li, T. J, J.W. Zhai, B. Shen, H.R. Zeng, Exploring novel bismuth-based materials for energy storage applications, J. Mater. Chem. C 6 (2018) 7976–7981.
[36] J. Yin, Y.X. Zhang, X. Lv, J.G. Wu, Ultrahigh energy-storage potential under low electric field in bismuth sodium titanate-based perovskite ferroelectrics, J. Mater. Chem. A 6 (2018) 9823–9832.
[37] T. Wang, L. Jin, Y. Tian, L.L. Shu, Q.Y. Hu, X.Y. Wei, Microstructure and ferroelectric properties of Nb_2O_5-modified $BiFeO_3$-$BaTiO_3$ lead-free ceramics for energy storage, Mater. Lett. 137 (2014) 79–81.
[38] D.W. Wang, Z.M. Fan, D. Zhou, A. Khesro, S. Murakami, A. Feteira, Q.L. Zhao, X.L. Tan, I.M. Reaney, Bismuth ferrite-based lead-free ceramics and multilayers with high recoverable energy density, J. Mater. Chem. A 6 (2018) 4133–4144.
[39] D.W. Wang, Z.M. Fan, W.B. Li, D. Zhou, A. Feteira, G. Wang, S. Murakami, S.K. Sun, Q.L. Zhao, X.L. Tan, I.M. Reaney, High energy storage density and large strain in Bi($Zn_{2/3}Nb_{1/3}$)O_3-doped $BiFeO_3$-$BaTiO_3$ ceramics, ACS Appl. Energy. Mater. 1 (2018) 4403–4412.
[40] E. Sapper, N. Novak, W. Jo, T. Granzow, J. Rödel, Electric-field-temperature phase diagram of the ferroelectric relaxor system (1-x)$Bi_{1/2}Na_{1/2}TiO_3$-x$BaTiO_3$ doped with manganese, J. Appl. Phys. 115 (2014) 194104.
[41] W.L. Zhao, R.Z. Zuo, J. Fu, Temperature-insensitive large electrostrains and electric field induced intermediate phases in (0.7-x)Bi($Mg_{1/2}Ti_{1/2}$)O_3-xPb($Mg_{1/3}Nb_{2/3}$)O_3-0.3$PbTiO_3$ ceramics, J. Eur. Ceram. Soc. 34 (2014) 4235–4245.